Accepted by the ApJ
Preprint typeset using LaTeX style emulateapj v. 01/23/15

arXiv:1512.00461v1 [astro-ph.GA] 1 Dec 2015

Down-the-barrel and transverse observations of the Large Magellanic Cloud: evidence for a symmetric galactic wind on the near and far sides of the galaxy*

K. A. Barger[1,2], N. Lehner[2], and J. C. Howk[2]

Accepted by the ApJ

ABSTRACT

We compare the properties of gas flows on both the near and far side of the Large Magellanic Cloud (LMC) disk using *Hubble Space Telescope* UV absorption-line observations toward an AGN behind (transverse) and a star within (down-the-barrel) the LMC disk at an impact parameter of 3.2 kpc. We find that even in this relatively quiescent region gas flows away from the disk at speeds up to ~100 km s^{-1} in broad and symmetrical absorption in the low and high ions. The symmetric absorption profiles combined with previous surveys showing little evidence that the ejected gas returns to the LMC and provide compelling evidence that the LMC drives a global, large-scale outflow across its disk, which is the likely result of a recent burst of star formation in the LMC. We find that the outflowing gas is multiphase, ionized by both photoionization (Si II and Si III) and collisional ionization (Si IV and C IV). We estimate a total mass and outflow rate to be $\gtrsim 10^7$ M$_\odot$ and $\gtrsim 0.4$ M$_\odot$ yr^{-1}. Since the velocity of this large-scale outflow does not reach the LMC escape velocity, the gas removal is likely aided by either ram-pressure stripping with the Milky Way halo or tidal interactions with the surrounding galaxies, implying that the environment of LMC-like or dwarf galaxies plays an important role in their ultimate gas starvation. Finally we reassess the mass and plausible origins of the high-velocity complex toward the LMC given its newly-determined distance that places it in the lower Milky Way halo and sky-coverage that shows it extends well beyond the LMC disk.

Keywords: galaxies: Magellanic Clouds - galaxies: dwarf - Galaxy: evolution - Galaxy: halo - ISM: individual (Large Magellanic Cloud)

1. INTRODUCTION

The Large Magellanic Cloud (LMC) is the nearest disk galaxy at 50 kpc away (see Walker 1999 and references therein) with a stellar and total mass of $M_\star \approx 3 \times 10^9\ M_\odot$ and $M_{\rm total} \approx 10^{10}\ M_\odot$, respectively (van der Marel et al. 2009) and a luminosity of $L = 0.2\ L^*$ (van der Marel et al. 2002). The LMC provides a closeup and relatively unobstructed view of another galaxy's interstellar medium (ISM) and of the processes influencing it. Galaxy interactions with the Small Magellanic Cloud (SMC; $M_{\rm SMC} \approx 1/10\ M_{\rm LMC}$; Kallivayalil et al. 2006 and Besla et al. 2010)—and possibly the Milky Way (MW; $M_{\rm MW} \approx 100\ M_{\rm LMC}$; e.g., Gardiner & Noguchi 1996, Boylan-Kolchin et al. 2013, and Kafle et al. 2014)—have stirred the gas and stars in these galaxies, stripped material from them (e.g., Putman et al. 1998), and triggered intense star formation in them (e.g., Harris & Zaritsky 2009). The stellar activity in these star-forming regions is thought to drive energetic winds and turbulance that distort the ISM (e.g., Stanimirović et al. 2004, Kim et al. 2003, Staveley-Smith et al. 2003, Danforth & Blair 2006, and Kim & Ostriker 2015).

Absorption line studies utilizing *Hubble Space Telescope (HST)* and the *Far Ultraviolet Spectroscopic Explorer (FUSE)* show gas with velocities consistent with material flowing away from this galaxy toward stars embedded within the LMC disk (Howk et al. 2002 and Lehner & Howk 2007, and Pathak et al. 2011). These absorption lines probe only the material foreground to the background stars. If a large-scale outflow is being driven from the LMC, gas should flow from both the near and far sides of the galaxy. We now have probes of gas flowing out of the backside of the LMC. To test if there is an outflow emanating from both sides of the LMC, in this paper we compare the absorbing material on the near and far side of this galaxy's disk along two neighboring sight lines as shown in Figure 1. Located behind the LMC, the sight line to the AGN CAL F penetrates through the entire disk, probing the regions in front, within, and behind the LMC. Embedded within the disk, the sight line to the star HD 33133 is only sensitive to the material in its foreground. Figure 2 illustrates the line-of-sight path to these targets. The absorption along these sight lines enable us to differentiate between the gaseous flows on both sides of the disk, since they lie only 7.2′ apart (a projected distance of 105 pc). These sight lines essentially probe the same environment within the disk (Figures 1–2).

Our experiment is analogous to combining the "down-the-barrel" galaxy absorption experiments, which probe only gas in the foregrounds of the integrated light from distant galaxies (e.g., Weiner et al. 2009, Rubin et al. 2010, 2014, Erb et al. 2012), and QSO absorption line experiments, which probe gas in both the foreground and background of the galaxy (e.g., Tumlinson et al. 2011, Kacprzak et al. 2011, Stocke et al. 2013, Wakker & Savage 2009, Lehner et al. 2015). In our case, our foreground probe is a single star, while the foreground and background probe is an AGN at an impact parameter of ~ 3.2 kpc from the optical center of the LMC (2.5 kpc from the kinematic center; Kim et al. 1999). Kacprzak et al. (2014) have also presented a joint comparison of the foreground absorption toward a galaxy with the foreground and background absorption from the same galaxy as seen toward a QSO, albeit in this case projected 58 kpc from the galaxy. In our experiment, the AGN lies behind the optical disk of the

[1] Department of Physics & Astronomy, Texas Christian University, Fort Worth, TX 76129, USA
[2] Department of Physics, University of Notre Dame, Notre Dame, IN 46556 , USA

* Based on observations made with the NASA/ESA *Hubble Space Telescope*, obtained at the Space Telescope Science Institute, which is operated by the Association of Universities for Research in Astronomy, Inc. under NASA contract No. NAS5-26555.

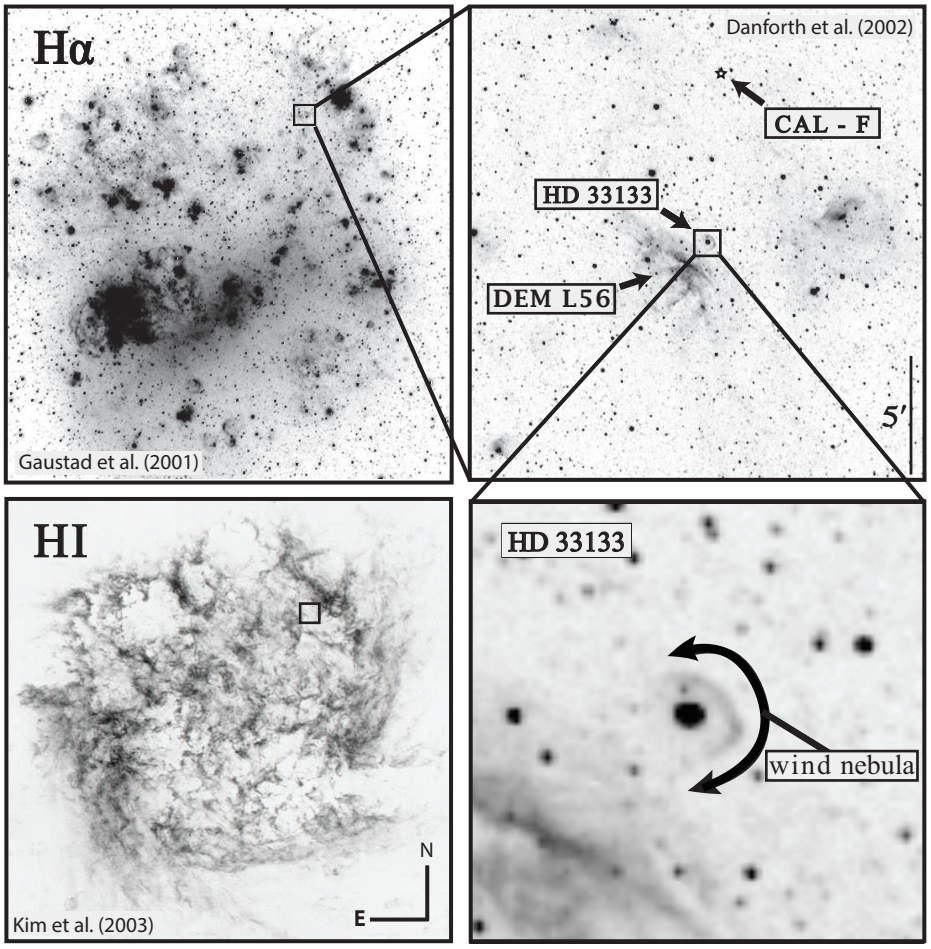

Figure 1. The global Hα and H I gas distribution of the LMC (left panels) and magnified Hα emission of the region surrounding the HD 33133 and CAL F sight lines at an impact parameter of $\sim$ 3.2 kpc from the optical center of the LMC (right panels). Surrounding HD 33133 is a wind nebula produced by the strong stellar winds emanating from this WR star. To the south east of this star lies the faint HII region DEM L56. The global H I and Hα maps are adapted from Figure 3 of Kim et al. (2003) using data from the Australia Telescope Compact Array (ATCA) and Parkes telescopes LMC survey and the South Hα Sky Survey Atlas (SHASSA: Gaustad et al. 2001). The right panels are adapted from images taken by Danforth et al. (2002).

LMC (similar to the QSO experiment of Bowen et al. 2005).

The HD 33133 and CAL F sight lines investigated in this study probe a relatively quiescent region of the galaxy known as the "Blue Arm" that has a star-formation rate (SFR) of $\mathrm{SFR_{Blue\ Arm}} \lesssim 0.03\ M_\odot\ \mathrm{yr^{-1}}$ compared to the LMC's total rate of $\mathrm{SFR_{LMC}} \lesssim 0.2\ M_\odot\ \mathrm{yr^{-1}}$ (or $\mathrm{sSFR} = 2 \times 10^{-11}\ \mathrm{yr^{-1}}$) (Harris & Zaritsky 2009 and van der Marel et al. 2009), allowing us to determine if the outflows observed in the Howk et al. (2002), Lehner & Howk (2007), and Pathak et al. (2011) studies persists throughout the LMC. However, it is important to note that although the Blue Arm is much less active today, it did undergo a major star formation event 100–160 Myr ago that formed the equivalent of five times the mass of the 30 Doradus' stellar population (Harris & Zaritsky 2009).

This paper is organized as follows. In Section 2, we discuss the UV spectroscopic absorption observations and their reduction. We examine the properties of the absorbing material in Section 4.2. We discuss the potential causes for the broad absorption that extends roughly 100 km s^{-1} off the H I disk along the HD 33133 and CAL F sight lines in Section 4, which includes a rotating thick disk, tidal debris, and a large-scale, feedback-driven wind. Finally, we conclude with our major results in Section 5.

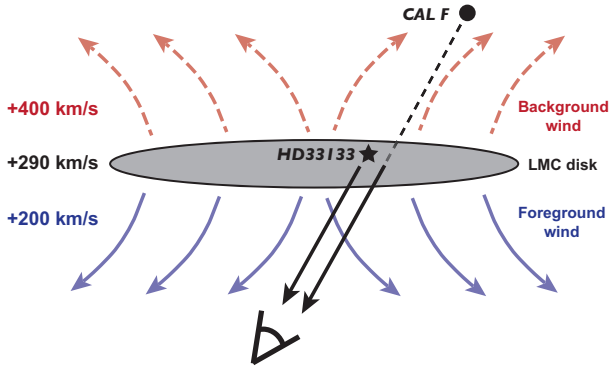

Figure 2. Schematic of the line-of-sight path to the star HD 33133 positioned within the LMC disk and the background AGN CAL F. Solid lines are used for the regions in front of the galaxy and dashed lines for the regions behind. Toward both sight lines, we detect neutral and ionized gas that extends much further than the H I velocity extent of the LMC disk. The kinematics and properties of the absorption along these sight lines are consistent with material flowing away from both sides of the galaxy's disk (see Section 4.2 below). The colored arrows illustrate the blue- and red-shifted gas distribution about the LMC in a large-scale galactic wind scenario.

2. OBSERVATIONS, REDUCTION, AND ANALYSIS

To determine the origin of the gas flowing away from the LMC, we examine the spectroscopic differences along two neighboring sight lines: an early-type star in the disk of the LMC and a background AGN. The details of the stellar HD 33133 and AGN CAL F targets are listed in Table 1 and their positions in the disk is shown in Figure 1.

CAL F was observed with COS G130M and G160M and the star HD 33133 with STIS E140M (through the square aperture to maximize throughput) with a wavelength coverage of 11340-1796 Å for COS and 1170 – 1730 Å for STIS. In these wavelength ranges, some or all of the following species are covered: O I λ1302, C II λ1334, C IV $\lambda\lambda$1548, 1550, N V $\lambda\lambda$1238, 1242, S II $\lambda\lambda$1250, 1253, 1259, Si II λ1190, 1193, 1260, 1304, 1526, Si III λ1206, Si IV $\lambda\lambda$1393, 1402, Al II λ1670, Fe II λ1608. In Table 2, we provide the observation summary for our program. We also use the *FUSE* observations of HD 33133 to explore the O VI λ1031 absorption; we refer the reader to Howk et al. (2002) for the data reduction of the *FUSE* data and the removal of the H_2 contamination from the O VI absorption.

Information about COS and COS data reduction can be found in Froning & Green (2009), Green et al. (2012), and Holland & et al. (2014). Information about STIS can be found in the STIS *HST* Instrument Handbook (Bostroem & Proffitt 2011). Standard reduction and calibration procedures were used to reduce the STIS and COS data. The alignment of the individual spectra was achieved through a cross-correlation technique in wavelength space. The individual exposures (in flux units), gratings, and echelon orders were combined to produce a single spectrum. Each coadded spectrum was then shifted into the LSR velocity frame.[4] As the COS absolute wavelength calibration is somewhat uncertain (up to 15 – 20 km uncertainty), we made sure that the centroids of the Galactic H I 21-cm emission in that direction from the LAB survey (Kalberla et al. 2005) match those seen in the Galactic absorption of neutral and singly ionized species.

We then normalized the AGN and stellar continua with Legendre polynomials within roughly $\pm$1000 km s^{-1} from the absorption under consideration. For the AGN, we used typically Legendre polynomials with orders of $m \leq 3$. For the stellar continuum of HD 33133, we used values of m ranging between 2–8 depending on the continuum complexity of the studied transitions. In Figures 3 and 4, we show the normalized profiles of several species in different ionization levels. The LMC component studied in this work is highlighted by the grey shaded area. Note that strong O I airglow emission lines contaminate part of the O I λ1302 and Si II λ1304 absorption in the COS spectrum owing to its large aperture, but the LMC O I λ1302 component appears to be free of any contamination.

We use the apparent optical depth (AOD) method—described in Savage & Sembach (1991)—to convert the observed absorption to column densities. This method relates the observed flux (F_{obs}), the flux of the continuum (F_c), and the line strength ($f\lambda_0$) of ionic transitions to determine their apparent column density without prior knowledge of their component structure:

$$N_a(v) = \frac{3.768 \times 10^{14}}{f\lambda_0} \ln\left(\frac{F_c(v)}{F_{obs}(v)}\right) \frac{\mathrm{cm}^{-2}}{\mathrm{km\,s}^{-1}}, \quad (1)$$

where f is the oscillator strength and λ_0 is the rest wavelength of the line in units of Å. We use the atomic parameters listed in Morton (2003) for the UV transitions.

3. OBSERVED PROPERTIES OF THE LMC GAS

3.1. *H I Emission and Systemic Velocity toward CAL F and HD 33133*

The H I emission in the region surrounding the stellar HD 33133 and AGN CAL F sight lines spans $+250 \lesssim v_{\rm LSR} \lesssim +310$ km s^{-1} with the emission peaking near $v_{\rm LSR} \approx +282$ km s^{-1} (see Figures 5 and 6). We use the H I emission from the LMC to define the velocity extent of the neutral gas in its disk. The distribution of H I emission along these two sight lines is very similar with their peaks offset by only $\sim$ 8 km s^{-1} (see Figure 5, combined ATCA and Parkes H I observations). Unlike the absorption toward LMC disk stars, this emission traces the entire extent and kinematics of the disk, though it is less sensitive to the gas at the lowest densities than absorption-line studies. We adopt $v_{\rm LSR} \approx +282$ km s^{-1} as the systemic velocity of the LMC for this region of the galaxy and the velocity spread of the H I emission as a reference for the extent of the gaseous disk when identifying LMC intermediate-velocity clouds (IVCs) that span up to 100 km s^{-1} from the H I emission of LMC disk and the HVCs that span to even greater velocities. Although the ionized thick disk can extend over a wider range of velocities, the bulk of the neutral gas in the LMC disk resides at $+250 \leq v_{\rm LSR} \leq +310$ km s^{-1} (Figure 5).

3.2. *Comparison of the Kinematic Structure between CAL F and HD 33133*

The stellar HD 33133 and AGN CAL F sight lines have absorption features at $-50 \lesssim v_{\rm LSR} \lesssim +100$ km s^{-1} that trace the MW and absorption features at $v_{\rm LSR} \approx +130$ km s^{-1} that traces an HVC that covers the face of the LMC (Staveley-Smith et al. 2003 and Lehner et al. 2009) in common (see Figures 3 and 4). The absorption at $v_{\rm LSR} \approx +130$ km s^{-1} is less prominent along the CAL F sight line as the COS spectrograph has a velocity resolution that is $\sim$ 2.6× higher than the STIS spectrograph, though this absorption is still present in the C II λ1334, Si II λ1260, 1526, and Si III λ1206 ions. From the observed properties of this HVC in H I emission (Staveley-Smith et al. 2003) and in absorption (Lehner et al. 2009), this complex was likely produced through LMC outflow events as discussed later in Section 4.3 and in those studies.

Toward both sight lines, continuous absorption of the LMC extends roughly -100 km s^{-1} further than the H I disk emission to $v_{\rm LSR} \approx +175$ km s^{-1} (see Figure 8). Because the HD 33133 sight line is only sensitive to material in its foreground (see Figure 2), this absorbing material must be moving away from the near side of the LMC. Along the CAL F sight line, we detect extra absorption that is not seen toward HD 33133, which extends +90 km s^{-1} further than the H I emission to $v_{\rm LSR} \approx +415$ km s^{-1}, in neutral, low- and high-ionization species (see Figures 4 and 8). Since this gas is not detected along the HD 33133 sight line, it must lie behind and be moving away from the LMC. In the following sections, we will focus on the intermediate-velocity absorption that spans

[4] We use the kinematic definition of the LSR, where the solar motion moves at 20 km s^{-1} toward $(R.A., Dec)_{J2000} = (18^{\rm h}3^{\rm m}50.29^{\rm s}, +30°00'16.8'')$ throughout this study for both the absorption- and emission-line datasets.

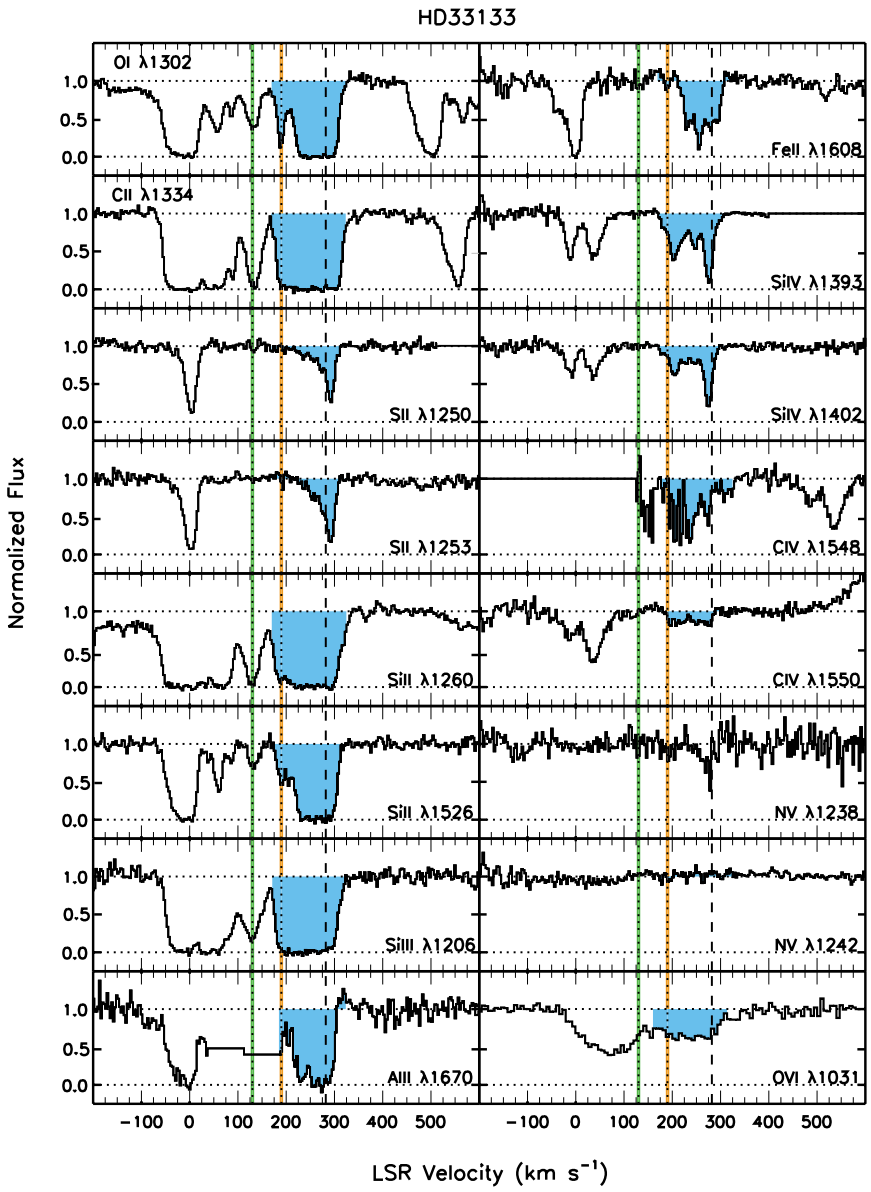

Figure 3. Normalized flux of HD 33133 as a function of the LSR velocity. The vertical dashed line at $v_{\rm LSR} = +282$ km s^{-1} indicates the peak velocity of the LMC HI emission, as illustrated in Figure 5, and the blue shaded region marks the extent of kinematically continuous gas within and around it from $+170 \lesssim v_{\rm LSR} \lesssim +325$ km s^{-1}. We indicate with the green vertical line an HVC at $v_{\rm LSR} = +130$ km s^{-1} that is part of the high-velocity cloud (HVC) complex toward the LMC (see Section 4.3 and Lehner et al. 2009) and the orange vertical line at $v_{\rm LSR} = +190$ km s^{-1} marks the wind nebula surrounding this star (see Figure 1). The absorption at $v_{\rm LSR} \lesssim 90$ km s^{-1} coincides with the disk and halo of the MW. The C II* λ1335 absorption of the MW is blended with the C II λ1334 transition of the LMC. The feature seen at $v_{\rm LSR} \approx +275$ km s^{-1} in the N V λ1238 panel is MW absorption from Mg II λ1239. All of these spectra were acquired with *HST*/STIS except the OVI λ1031 in the bottom-right panel, which was obtained with *FUSE*.

Table 1
Summary of Targets

Target	Alias	Type	(R.A., Dec)$_{\rm J2000}$
HD 33133	Sk–66°51, Br 13	WN8h star	($5^{\rm h}3^{\rm m}8.84^{\rm s}$, −66°40′57.30″)
CAL F	RX J0503.1−6634	Seyfert 1 ($z = 0.064$)	($5^{\rm h}3^{\rm m}3.93^{\rm s}$, −66°33′46.50″)

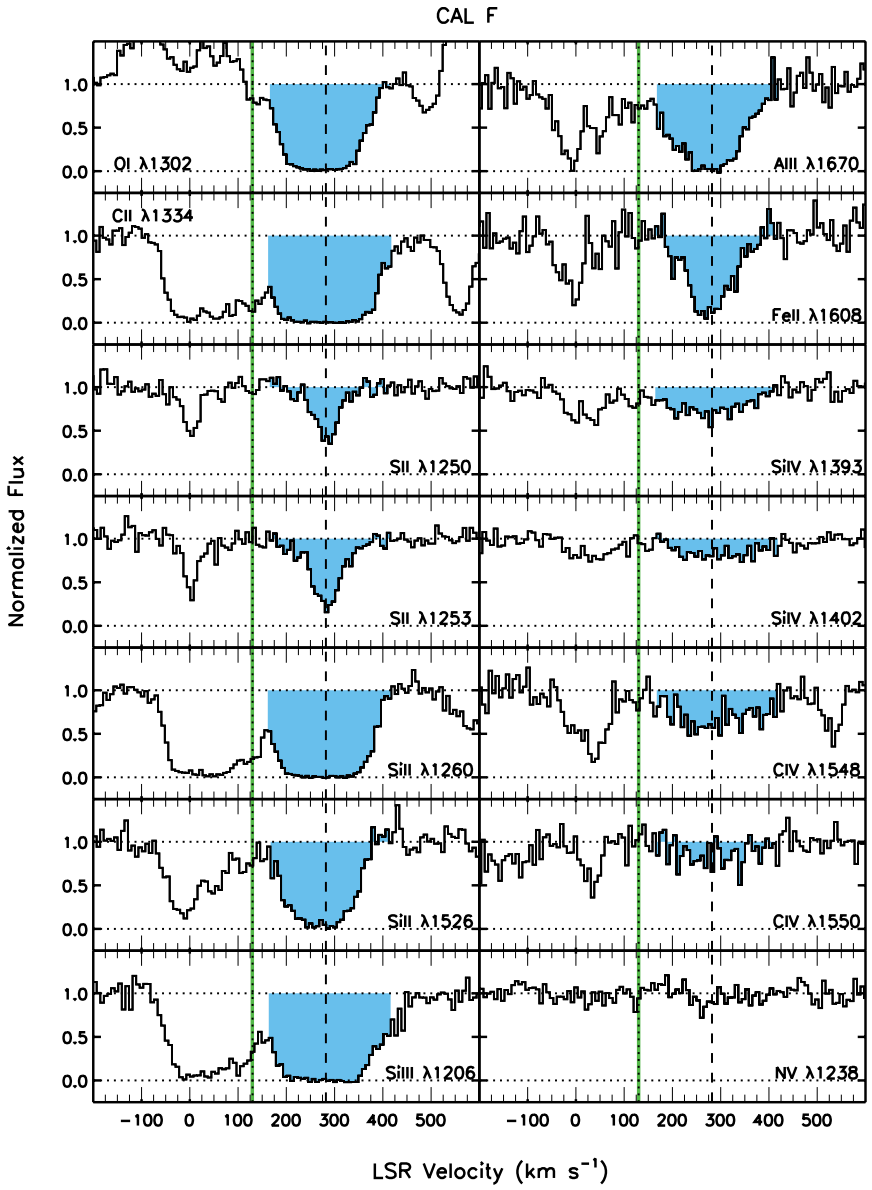

Figure 4. Normalized flux of CAL F as a function of the LSR velocity. The vertical dashed line at $v_{\rm LSR}$ = +282 km s^{-1} indicates the peak velocity of the LMC HI emission, as illustrated in Figure 5, and the blue shaded region marks the extent of kinematically continuous gas within and around it from +165 $\lesssim v_{\rm LSR} \lesssim$ +415 km s^{-1}. The green vertical line at $v_{\rm LSR}$ = +130 km s^{-1} marks an HVC complex in the direction of the LMC in the C II λ1334, Si II λ1260, 1526, and Si III λ1206 ions (the feature in S II λ1250 is unrelated as it is not observed in S II λ1253). The absorption at $v_{\rm LSR} \lesssim$ 90 km s^{-1} coincides with the disk and halo of the MW. The C II* λ1335 absorption of the MW is blended with the C II λ1334 transition of the LMC. The O I λ1302 is contaminated by strong O I airglow emission lines near $v_{\rm LSR}$ = −100, 0, and +550 km s^{-1}. The feature seen at $v_{\rm LSR} \approx$ +275 km s^{-1} in the N V λ1238 panel is MW absorption from Mg II λ1239. The LMC absorption along this sight line extends beyond $v_{\rm LSR} \approx$ +325 km s^{-1} absorption detected along the LMC HD 33133 disk star sight line (see Figure 3).

Table 2
Summary of Observations[a]

Target	Instrument	Aperture	Grating	$\lambda_{\rm center}$ (Å)	λ range (Å)	Resolution (km s^{-1})	Total $t_{\rm exp}$ (ks)
HD 33133	STIS	0.2″ × 0.2″	E140M	1425	1140–1735	6.5	2.8
CAL F	COS	2.4″	G130M	1291	1140–1430	17	4.7
CAL F	COS	2.4″	G160M	1600	1385–1750	17	4.0

[a] *HST* program ID 11692 (PI: Howk).

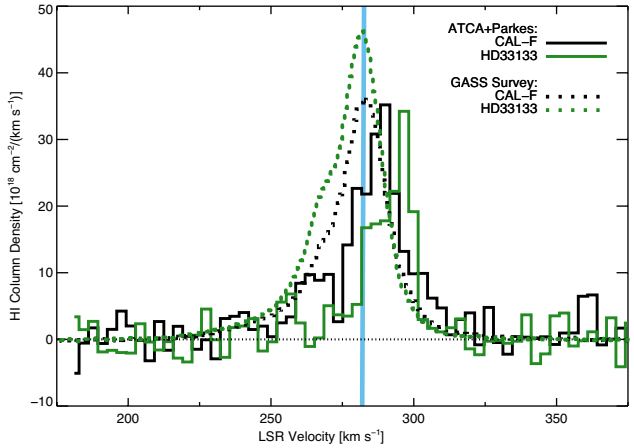

Figure 5. The H I gas distribution along the CAL F (black) and HD 33133 (green) sight lines. The LMC H I emission peaks at +288 km s^{-1} along the CAL F sight line and at +296 km s^{-1} towards HD 33133 when resolved at 1′ (ATCA and Parkes survey; Kim et al. 1998, 2003; Staveley-Smith et al. 2003). The H I of both sight lines peaks at +282 km s^{-1} (blue line) when resolved over a larger 16′ region (Parkes Galactic All-Sky Survey; McClure-Griffiths et al. 2009 & Kalberla et al. 2010).

up to roughly ±100 km s^{-1} off of the LMC. We discuss the LMC HVC and its origin in Section 4.3.

The absorption along the stellar HD 33133 sight line has an extra narrow component near $v_{\rm LMC} \approx -90$ km s^{-1} ($v_{\rm LSR} \approx +190$ km s^{-1}; Figures 3 and 8), as seen in O I, Si II, Si IV, and other ions, that coincides with an approaching shell wall of the wind nebula that surrounds this star as seen in the bottom-right panel of Figure 1 (Chu et al. 1999). In contrast, the Si IV and C IV absorption along the AGN CAL F sight line only consists of a broad absorption (see Figure 8). Although the AGN and stellar spectra have different resolutions (see Table 2), this does not drive the disparity in their velocity structure. As displayed in Figure 8, the STIS spectrum still shows the extra narrower component when smoothed and rebinned to the COS resolution and sampling. These narrow components indicate that the gas near the WR star HD 33133 is strongly affected by its presence. We discuss these components in more detail in the Appendix, but we emphasize their absence in the spectrum of CAL F, demonstrating that the region near CAL F is does not probe an H II or supershell region (see Figure 8).

3.3. *Ionization Properties of the LMC Gas Along CAL F*

The ionization ratios of the low- and high-ionization species along the CAL F sight line are strikingly uniform. As Figure 7 shows, the $N_{\rm Si\,II}/N_{\rm O\,I}$ and $N_{\rm C\,IV}/N_{\rm Si\,IV}$ ratios are consistently 1/5 and 3.5, respectively, over their combined $\sim$ 200 km s^{-1} velocity extent (at the H I disk velocities, O I and Si II are saturated). The uniformity of these ratios in the approaching and receding gas suggests the LMC's the near and far side gas flows have very similar properties and origins.

3.3.1. *Weakly ionized gas and ionization level*

To determine the ionization properties of the LMC component, we first compare the Si II and O I ions, tracers of the low ionization and neutral gas. As silicon and oxygen have similar nucleosynthetic evolution, only differences in ionization and depletion should affect the $N_{\rm Si\,II}/N_{\rm O\,I}$ ratio. However, because these elements are only mildly depleted in diffuse gas, [Si II/O I][5] provides constraints on the hydrogen ionization fraction (x(H$^+$); Zech et al. 2008). If [Si II/O I] > 0, then the gas is substantially ionized, as Si II traces both the neutral and ionized gas, whereas O I only traces the neutral gas. We find [Si II/O I] $= +0.50 \pm 0.08$ for the foreground and background intermediate-velocity gas surrounding the LMC; this implies an ionization fraction of x(H$^+$) $\geq 72\%$ for warm gas traced by the low-ionization species. Since highly-ionization states of silicon are not taken into account (esp. Si III), this is a strict lower limit on the total ionization fraction.

3.3.2. *Highly ionized gas*

The LMC gas along the AGN CAL F sight line is dominantly ionized with very broad absorption in the high ionization species as shown in Figure 8 for the C IV and Si IV apparent column density profiles. Since low and high ions and neutral gas are observed at similar velocities, the extended LMC absorption toward CAL F is multiphase. Unfortunately, the *FUSE* observations of the CAL F sight line have too low S/N to place any useful constraints on the O VI along this sight line. There are, however, good *FUSE* observations of the HD 33133 sight line. In Figure 9, we compare the O VI toward HD 33133 and C IV toward CAL F and between $-100 \lesssim v_{\rm LMC} \lesssim +25$ km s^{-1} and find that there is an excellent match in their kinematic structure with only some minor variations, which could in part be caused by uncertainty in the O VI continuum modeling (Howk et al. 2002). As the ionization potential of OVI is > 113 eV and the absorption in the high ions (C IV, Si IV, and O VI) is broad, this reinforces that the gas is multiphase and also strongly suggests that the high ions are tracing a hot extended gas flow as we further argue below. The Si IV and C IV along the HD 33133 sight line also likely have a broad underlying component structure that is blended with narrow components that are associated with a wind nebula and the photoionized gas that surrounds this WR star as further discussed in the Appendix, which is consistent with similarly blended broad and narrow profiles that Lehner & Howk (2007) found towards other LMC stars. As noted in Lehner & Howk (2007) and observed toward HD 33133, there are none of the O VI narrow component features that are observed in C IV or Si IV toward that star, implying that any O VI absorption from the wind nebula is negligible.

The absence of narrow components in the C IV and Si IV toward CAL F and O VI toward HD 33133 and the similarity between these O VI, C IV, Si IV profiles most certainly indicate that the high ionization species is collisionally ionized. Further insights can be gained from the ionic ratios. Over 200 km s^{-1} along the CAL F sight line, the LMC C IV and Si IV column density profiles match each other extremely well with $N_{\rm C\,IV}/N_{\rm Si\,IV} \approx 3.5$ (see Figure 7). The absence of variation in the $N_{\rm C\,IV}/N_{\rm Si\,IV}$ ratio strongly suggests that the same ionization processes affect the highly ionized gas over the entire velocity of the extended gaseous structures and the LMC's disk. While this is quite different from what is typically observed in the MW disk on several kiloparsec length-scale (Lehner et al. 2011), Lehner & Howk (2007) also noted a striking similarity between the $N_{\rm O\,VI}/N_{\rm C\,IV}$ ratios for the broad LMC and high-velocity components.

Only photoionization by a hot plasma or collisional ionization process (e.g., cooling hot gas, turbulent mixing layers, and fast radiative shocks) can produce such a high C IV/Si IV

[5] We use the familiar square-bracket notation [X/Y] = log (N$_X$/N$_Y$) − log $(X/Y)_\odot$, where the solar abundance is adopted from Asplund et al. (2009).

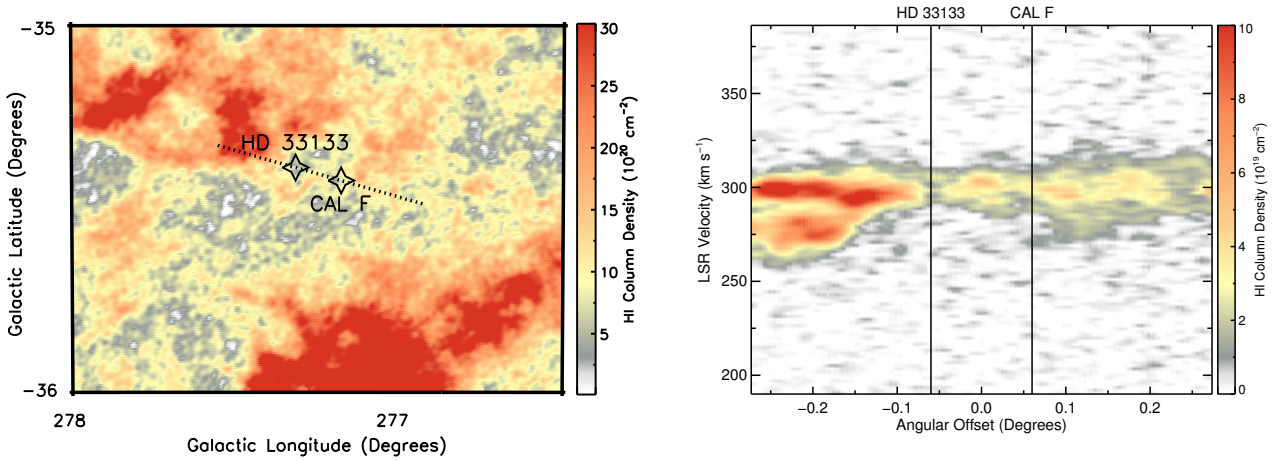

Figure 6. H I emission maps of the gas surrounding the HD 33133 and CAL F sight lines. The left figure shows a map of the H I emission integrated over the $+190 \leq v_{\rm LSR} \leq +385$ km s^{-1} range—the full range of the combined ATCA HI and Parkes telescopes LMC survey (Kim et al. 1998 and Kim et al. 2003). The right map shows a position-velocity diagram along the dotted line in the integrated H I map.

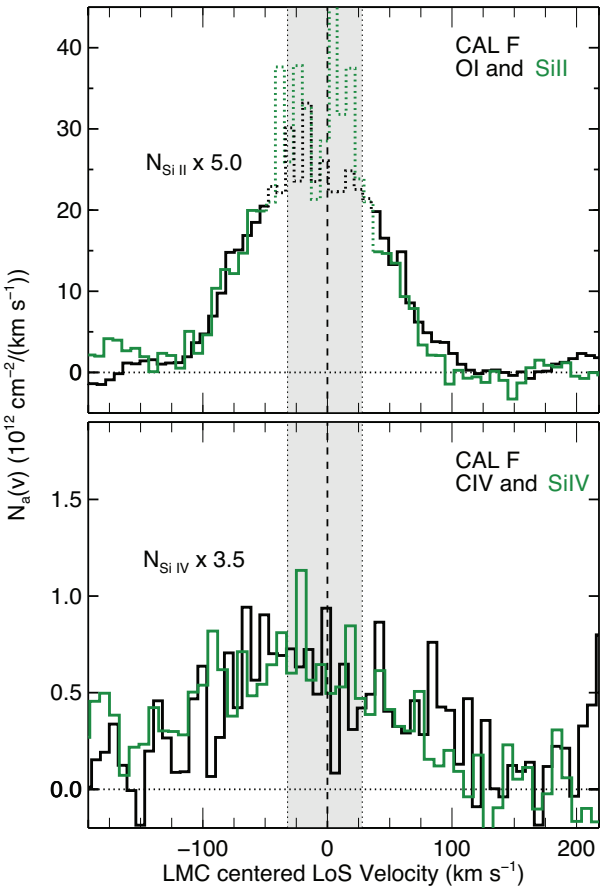

Figure 7. The apparent column densities of the low (top) and high (bottom) ionization species along the AGN CAL F sight line. These distributions are traced in green for the Si II and Si IV ions and in black for the O I and C IV ions. The dashed portions of the spectra are regions where the absorption is saturated. The extent of H I emission from the LMC disk is highlighted in light grey.

ratio (see models by Gnat & Sternberg 2007, 2009, Kwak & Shelton 2010, Oppenheimer & Schaye 2013, and observations by Knauth et al. 2003, Lehner et al. 2011). Further, assuming that the O VI absorption toward CAL F and HD 33133 is similar as the lie only a projected distance of 105 pc appart, we have $N_{\rm O\ VI}/N_{\rm C\ IV} \approx 2$ (see Fig. 9). This is inconsistent with photoionization by a hot plasma as this process produces ratios of $N_{\rm O\ VI}/N_{\rm C\ IV} \ll 1$ (see Knauth et al. 2003). Therefore the highly ionized LMC gas observed toward CAL F is hot and collisional ionized. Since the b-value of C IV is $\langle b \rangle = 84 \pm 9$ km s^{-1}, this would imply a temperature of 7×10^6K if the broadening was dominated by a single thermally broadened component. This is unrealistic since it would imply that the fraction of C IV/C or Si IV/Si is too small for the observed strong absorption of C IV or Si IV (see Oppenheimer & Schaye 2013). The broadening of the C IV and Si IV absorption must therefore be dominated by non-thermal motions or the result of several thermally broadened ($b_{\rm th} \approx 10$–15 km s^{-1}) components. The very symmetric high-ion kinematic profiles and absence of structures in the profiles strongly suggest that non-thermal motions is the main source of the broadening.

We discuss below the possible origin of this broad absorption and the inferred properties of the gas along the CAL F sight line as well as toward other sight lines throughout the LMC disk (see Howk et al. 2002 and Lehner & Howk 2007 for these other sight lines).

4. DISCUSSION

4.1. *Origin of the Extended LMC Absorption Toward CAL F*

The differences in the absorption along the CAL F and HD 33133 sight lines allow us to differentiate between the gas flows on the near and far side of the LMC. Although we do not know how far into the disk star HD 33133 lies, this sight line only probes foreground gaseous structures, whereas the AGN CAL F sight line also probes the material behind the galaxy. We find that predominantly ionized gas flows away from the H I disk at velocities up to $v_{\rm LMC} \approx -120$ km s^{-1} ($v_{\rm LSR} \approx +165$ km s^{-1}) on the near side of the LMC and $v_{\rm LMC} \approx +135$ km s^{-1} ($v_{\rm LSR} \approx +410$ km s^{-1}) on the far side

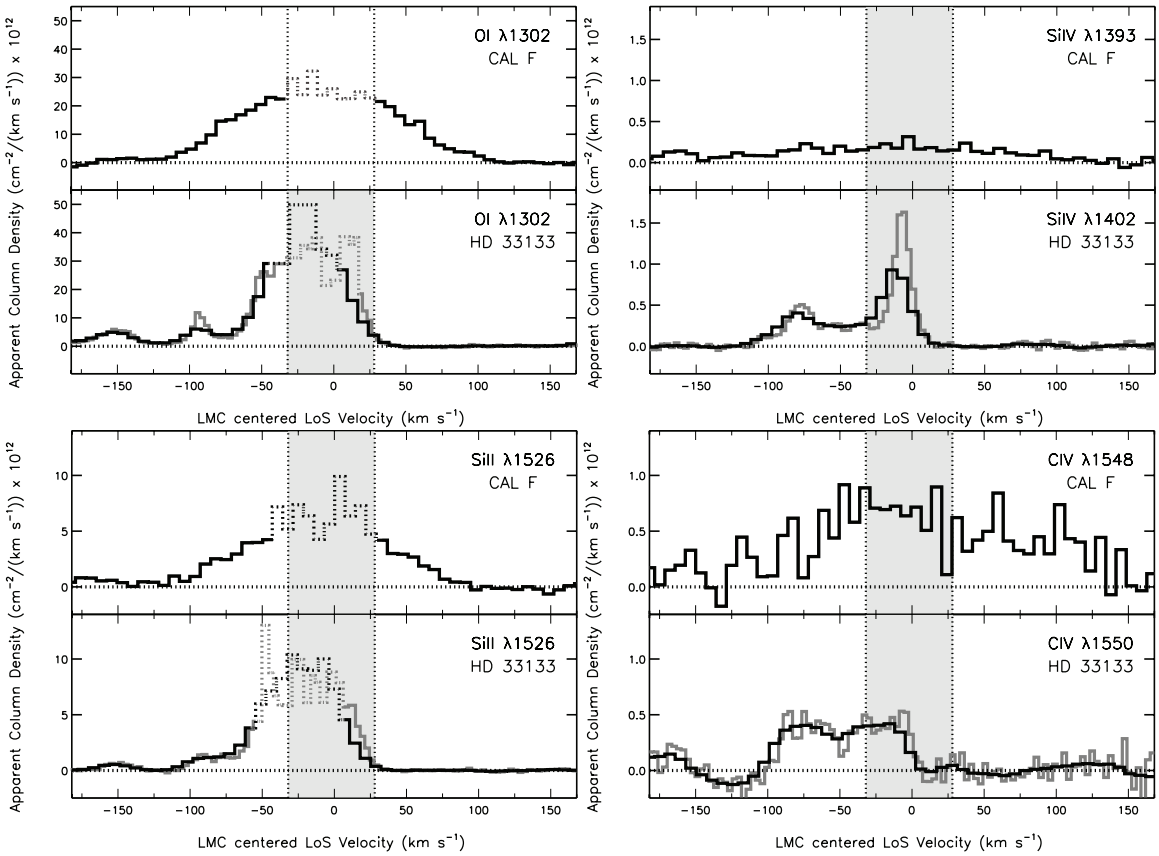

Figure 8. Comparison of the low- and high-ionization species of the HD 33133 (right) and CAL F (left) sight lines. The bottom panels show the full STIS 6.5 km s^{-1} resolution (grey) and smoothed to a 17.0 km s^{-1} resolution (black). The systemic velocity of the LMC at $v_{\rm LMC}$ = 0 km s^{-1} is defined to be at the peak position of the H I emission ($v_{\rm LSR}$ = +282 km s^{-1}). The extent of H I emission from the LMC disk is highlighted in light grey over the $-32 \le v_{\rm LMC} \le +28$ km s^{-1} ($+250 \le v_{\rm LSR} \le +310$ km s^{-1}) velocity range. The O I and Si II absorption saturates over $-57 \lesssim v_{\rm LMC} \lesssim +18$ km s^{-1}.

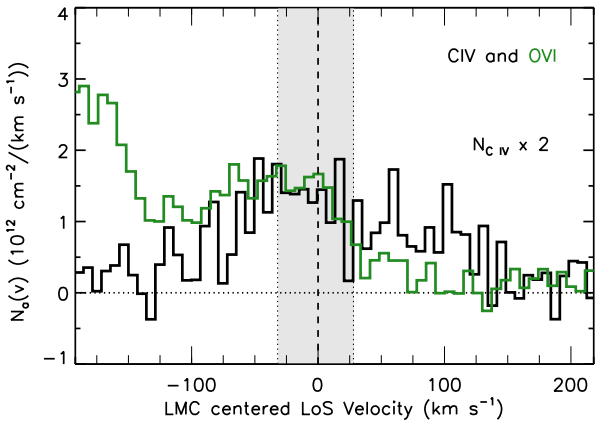

Figure 9. Comparison of C IV (black) apparent column density along the CAL F AGN sight line and of O VI (green) along the stellar HD 33133 sight line. The *FUSE* O VI spectrum, with a velocity resolution of ~ 15 km s^{-1}, has been rebinned to match the C IV spectrum acquired with COS a 17.0 km s^{-1} resolution. The O VI absorption at $v_{\rm LMC} \lesssim -100$ km s^{-1} probes the Galactic halo. The extent of H I emission from the LMC disk is highlighted in light grey.

of the LMC along the CAL F sight line. Across the face of the galaxy, Howk et al. (2002) and Lehner & Howk (2007) detected multiphase IVC gas on the near side of the LMC towards 19 sight lines. Within 100 km s^{-1} of the LMC's disk, the IVC absorption is relatively continuous. Multiple processes could produce these gas structures, including a lagging thick disk, tidally disrupted gas, and galaxy outflows. Here we discuss the likelihood of each of these origins for the LMC IVC gas that extends ~ 100 km s^{-1} off both sides of the LMC's H I disk as shown in Figure 8. In the Appendix, we discuss the origin of the LMC HVC at $v_{\rm LMC} \lesssim -150$ km s^{-1}.

In many galaxies, a rotating thick disk gas lags behind the rotation of a thin disk (see Sancisi et al. 2008 and references therein). This lag has been observed as an offset of the thick disk rotation with respect to the thin disk at the same projected radial distance, sometimes including a gradient in velocity with height. This lag has been observed in both neutral gas (e.g., Oosterloo et al. 2007) and ionized gas (e.g., Heald et al. 2007 and Kamphuis et al. 2007). The kinematic differences between the thin disk, the thick disk, and any extended gas structures will cause the absorption from these structures to span different, and often larger, velocity ranges.

Any effects of differential rotation between thin disk and out of disk structures have a maximum observation signature for edge on galaxies, those with inclination angles that approach $i = 90°$. The LMC is viewed nearly face on, with an inclination angle of only $i = 22°$ (derived for the H I disk gas at the position of our sight lines of interest; Kim et al. 1998). Because the line-of-sight projection of the azimuthal motions scale with $\sin i$, the HD 33133 and CAL F observations are not very sensitive to the differences in azimuthal motions between its thin and thick disk. Kim et al. (1998) measured the maximum rotational motion of the H I gas in the LMC

to be $v_{\rm rot,\ max} = 65$ km s^{-1}. If the vertical velocity dispersion of the ionized gas in the thick disk is roughly 10 – 25% of the maximum rotational velocity of the LMC, then the lag along the line of sight would translate to a broadening of only 3 – 6 km s^{-1}. Therefore, the spectral broadening due to a lagging thick disk is negligible.

Galaxy interactions between the MCs—and possibly the MW—have displaced over two billion solar masses of both neutral and ionized gas from the Magellanic Clouds, which now lies in the Leading Arm, Magellanic Bridge, and the Magellanic Stream (e.g., Putman et al. 1998; Brüns et al. 2005; Lehner et al. 2008, 2009; Barger et al. 2013, 2014; Fox et al. 2014). Through component fitting of kinematically resolved H I observations, Nidever et al. (2008) found that two major filamentary structures in this tidal debris could be traced back to the bridge connecting these two galaxies and the 30 Doradus starburst region of the LMC. The filament that crosses the LMC has a velocity very similar to that of the galaxy. The HD 33133 and CAL F sight lines, however, lie far from these filamentary structures and have a much wider kinematic extent; therefore the high-velocity absorption along these sight lines is likely unassociated with the major tidal structures that are protruding from the LMC. Further, tidal processes are unlikely to produce such symmetric velocity profiles (see Section 3.2) and ionization properties (see Section 3.3) as observed for gas on the near and far side of the LMC.

Neither a thick disk that lags behind a thin disk nor a tidal structure that projects out of the disk can produce the absorption signatures that extend ~ 100 km s^{-1} beyond the H I disk of the LMC. Because of the similar kinematics and ionization properties of the outflowing gas on the near side and far side of the galaxy, and because of the similarities they share with the widespread outflows found by Howk et al. (2002) and Lehner & Howk (2007) on the near side of the LMC, we conclude that a large-scale wind driven by the cumulative star formation of the LMC has expanded across much of the galaxy. The lack of stellar sight lines that show signatures of inflows signifies that gas recycling through galactic fountain processes is likely inefficient (Howk et al. 2002, Lehner & Howk 2007, and Lehner et al. 2009), presumably because the ejected gas is more susceptible to ram-pressure stripping by the Galactic halo and tidal processes as it lies further from the center-of-mass of the LMC (see the recent works by Hammer et al. 2015 and Salem et al. 2015 for evidence of ram pressure effects exerted by the hot gas in the Milky Way on the Magellanic system).

4.2. *Properties of the LMC Outflows*

Along the AGN CAL F and LMC disk star HD 33133 sight lines, we detect broad absorption that spans ± 100 km s^{-1} around the H I emission from the LMC's disk (illustrated in Figure 8). By comparing the kinematics along these sight lines, in Section 3.1 we showed that this gas is moving away from both sides of this galaxy at speeds up to 100 km s^{-1} (Section 3.1). The properties of the gas flows on both sides of the disk are also similar in the ionization fraction of the low-ionization species (Section 3.3) and the collisional ionization processes that are ionizing the high ionization species (Section 3.2). These similarities suggest that gas on the near and the far side may have the same origin.

Much of this outflowing gas could escape from the LMC if it reaches velocities in excess of $\sim 2^{1/2}$ times greater than the maximum rotational velocity of the galaxy (e.g., see Heckman et al. 2000). If the outflows along the HD 33133 and CAL F sight lines are perpendicular to the H I disk, then the expelled gas velocities could exceed ~ 110 km s^{-1} (correcting for the line-of-sight projection), potentially enough for some of this gas to escape ($v_{\rm esc} \approx 90$ km s^{-1} with $v_{\rm rot,\ max} = 65$ km s^{-1} for the H I; Kim et al. 1998). Even more gas could escape when combined with tidal and ram-pressure stripping processes. These outflows could drive gas far above the galaxy's disk to create large, gaseous complexes around the LMC that feed the MW halo.

To estimate the baryonic and metal masses and flow rates of the LMC outflows, we proceed as follows. At a given radius (R), this mass is the product of the average particle mass (μ), the column density perpendicular to the disk of the LMC ($N_\perp = N_{\rm obs} \cos i$), and the surface area ($A = \Omega f_\Omega R^2$) of the outflow, where Ω is the solid angle subtended by the wind with a covering fraction f_Ω; this follows a similar procedure used by Fox et al. (2007). The high detection rate of these outflows in active and quiescent regions of the LMC as found by Howk et al. (2002), Lehner & Howk (2007), Pathak et al. (2011), and this study indicate that this intermediate-velocity gas covers most of the galaxy. For simplicity, we assume that $f_\Omega = 1$. For comparison, Lehner et al. (2009) found $f_\Omega = 0.7$ for the low-ionization species and $f_\Omega = 0.9$ for the high-ionization species of the HVC complex in the foreground of the LMC. Readily-identifiable winds observed in other galaxies typically have a biconical structure as they are often produced in the central regions of the galaxies where high concentrations of star formation and AGN activity occur (e.g., Heckman et al. 1990; Slavin et al. 1993; Veilleux et al. 1994). However, in the LMC, the galactic winds are likely pervasive throughout the disk as a result of its wide spread star formation; we therefore, conservatively, adopt $\Omega = 2\pi$ when calculating the mass loss due to these outflows:

$$M_{\rm out} \approx \mu\ N_{\rm H\perp}\ 2\pi\ R_{\rm out}^2. \tag{2}$$

If the ejected material travels at a constant velocity, then the rate ($\dot{M} = dM/dt$) at which the gas leaves the galaxy is given by:

$$\dot{M}_{\rm out} \approx \mu\ N_{\rm H\perp}\ 4\pi\ R_{\rm out}\ v_{\rm out}, \tag{3}$$

where $R_{\rm out} = v_{\rm out}\ t$.

To estimate the mass that has been ejected from the LMC and the corresponding rate at which it leaves the disk, we assume that the material has reached a distance equal to the H I radius of LMC's disk ($R = 3.7$ kpc; Kim et al. 1998) and that it travels at an outward velocity of $v_{\rm out} = 50$ km s^{-1} (roughly half of the full extent of the continuous intermediate-velocity absorption). These assumptions translate into an outflow time period of 75 Myrs.

We adopt the following assumptions to estimate the mass of the baryons and metals that the LMC is losing into its surroundings and their corresponding rates: (1) An ionization fraction of 72% for the gas traced by the low-ionization species; in Section 3.3, we found that $x(\mathrm{H}^+) \geq 0.72$ based on comparisons of the O I and Si II ions. (2) An ionization fraction of 100% for the gas traced by the high-ionization species Si IV and C IV. (3) An average particle mass of $\mu \approx 1.3 m_{\rm H}$ to account for the contribution of He when determining the total baryon mass in a given phase. And (4) a metallicity equal to that of the present-day LMC ($Z = 0.5\ Z_\odot$; Russell & Dopita 1992); as this material is likely associated with feedback from active-stellar regions, this metallicity is a lower limit (but it is unlikely to be much larger than a factor 2-3). We integrate the

Table 3
Component Summary of the Ionization Species along the CAL F sight line

Ion Transition	$\log N_{\rm ion}/\,{\rm cm}^{-2}$ $[-117, -32]$[a]	$\log N_{\rm ion}/\,{\rm cm}^{-2}$ $[+33, +128]$[a]
O I λ1302	> 15.13	> 14.84
Si II λ1526	> 14.47	14.20 ± 0.04
Si III λ1206	> 13.79	> 13.68
Si IV λ1393	13.14 ± 0.04	13.02 ± 0.04
Si IV λ1402	12.94 ± 0.12	13.10 ± 0.09
C IV λ1548	13.60 ± 0.07	13.78 ± 0.05
C IV λ1550	$13.47^{+0.13}_{-0.20}$	13.89 ± 0.08

[a] Integration range (in $\rm km\,s^{-1}$) in the LMC frame. This corresponds to $+165 \le v_{\rm LSR} \le +250\ \rm km\,s^{-1}$ and $+315 \le v_{\rm LSR} \le +410\ \rm km\,s^{-1}$.

absorption profiles $-117 \le v_{\rm LMC} \le -32\ \rm km\,s^{-1}$ (near side) and $+33 \le v_{\rm LMC} \le +128\ \rm km\,s^{-1}$ (far side) to estimate the column densities of this wind along the CAL F sight line and list them in Table 3 for select low- and high-ionization species.

We use the Si II and Si III ions to determine the mass of the gas flowing from LMC in the neutral and low-ionization phases. Nearly all of the silicon exists in these low-ionization states (i.e., $(N_{\rm Si\,II} + N_{\rm Si\,III})/N_{\rm Si} \approx 1$). These ions have an average column density (over the near and far side of the LMC) of $\log(\langle N_{\rm Si\,II}\rangle + \langle N_{\rm Si\,III}\rangle) > 14.42$ (see Table 3), where we integrated Equation (1) over the velocity interval defined in Table 3 to estimate $N_{\rm obs}$. We use the $\langle N_{\rm H}\rangle = \sum\langle N_{\rm Si}\rangle\,(Z/Z_\odot)^{-1}\,({\rm Si/H})_\odot^{-1}$ to convert these column densities into total hydrogen column density ($\log(N_{\rm H_{total}}) \ge 19.22$) and Equations (2) and (3) to calculate the corresponding outflow masses and outflow rates. The mass loss contribution for the low-ionization phases is given by:

$$M_{\rm gas,\ low} = 1.3 m_{\rm p} \frac{(\langle N_{\rm Si\,II}\rangle + \langle N_{\rm Si\,III}\rangle)\ \cos i}{Z/Z_\odot\ ({\rm Si/H})_\odot}\ 2\pi R^2 \qquad (4)$$

To determine the mass contribution of the high-ionization species ($M_{\rm gas,\ high}$), we use Si IV. The broad component structure of the Si IV line and the $N_{\rm C\,IV}/N_{\rm Si\,IV} \approx 3.5$ along the CAL F sight line indicate that Si IV probes collisionally ionized gas (see Sections 3.2 and 3.3). The average column density of this ion along both sides of the LMC disk is $\log(\langle N_{\rm Si\,IV}\rangle) = 13.05 \pm 0.03$ (see Table 3). However, because silicon will also exist in higher-ionization states, this calculation must also convert the fraction of silicon that exists in the Si IV state to the total silicon in all high-ionization states (i.e., $N_{\rm Si,\ high} = \langle N_{\rm Si\,IV}\rangle (N_{\rm Si\,IV}/N_{\rm Si})^{-1}$). Through photoionization and collisional ionization models, Oppenheimer & Schaye (2013) found a maximum Si IV ionization fraction of $N_{\rm Si\,IV}/N_{\rm Si} = 0.4$—although this value could be a factor 6 lower for a wide range of typical temperatures. We adopt this maximum ionization fraction when calculating $N_{\rm Si}$, which places a strict lower limit on the total mass loss when converted to $N_{\rm H}$.

Galactic winds that are driven by stellar activity that expels metal enriched gas into and out of the galaxy. To similarly convert from the silicon column densities to metals, we assume that $(m_{\rm Si}/m_{\rm Metals})_\odot = 0.064$ for solar mass fraction of metals in silicon (Asplund et al. 2009), where $\mu_{\rm Si} = 28\ m_{\rm H}$ (see Peeples et al. 2014 and Lehner et al. 2015 for more details on this procedure):

$$M_{\rm Z,\ total} = 28 m_{\rm p} \frac{(\langle N_{\rm Si\,II}\rangle + \langle N_{\rm Si\,III}\rangle + \langle N_{\rm Si\,IV}\rangle)\ \cos i}{(m_{\rm Si}/m_{\rm Metals})_\odot}\ 2\pi R^2 \qquad (5)$$

Table 4
Summary of Outflow Masses and Rates[a]

	Gas Phase	M $(10^6\ M_\odot)$	$\dot{M}$ $M_\odot/\,{\rm yr}^{-1}$
Baryons	Low Ions	$\gtrsim 14.6$[b]	$\gtrsim 0.41$
Baryons	High Ions[c]	> 1.4[e]	$> 4.0\times10^{-2}$[d]
Metals	Low- & High-Ions	$> 8.0\times10^{-2}$	$> 2.2\times10^{-3}$

[a] We assume that these winds reach a distance of 3.7 kpc and are moving at a rate of $50\ \rm km\,s^{-1}$. We also assume a present-day LMC metallicity of $Z = 0.5\ Z_\odot$ (Russell & Dopita 1992); if these outflows are associated with stellar feedback, then they could be enriched by as much as 2 – 3 times more metals. These values are therefore conservative estimates.
[b] Gas probed by Si II and Si III. Both of these ions are saturated near LMC disk velocities.
[c] For the photoionized and collisionally ionized gas probed by Si IV.
[d] If we use C IV instead of Si IV to calculate M and $\dot{M}$ in the highly ionized phase, where $N_{\rm C\,IV}/N_{\rm C}$ is assumed to be < 0.3 (the maximum expected value for collisionally and photoionized gas; see Gnat & Sternberg 2007) and ${\rm C/H} = 10^{-4}$ (Kurt & Dufour 1998), we find $0.7\times10^6\ M_\odot$ and $0.02\ M_\odot/\,{\rm yr}^{-1}$.

These mass losses and their corresponding rates are listed in Table 4.

We find that the galactic outflows of the LMC have ejected at least $1.6\times10^7\ {\rm M}_\odot (R_{\rm out}/3.7\ {\rm kpc})^2$ of gas from its disk. For comparison, Fox et al. (2014) found that tidal interactions have removed more than $2.0\times10^9\ {\rm M}_\odot$ in neutral and ionized gas from both of the Magellanic Clouds. Although we find that the mass of the LMC's outflow is 100 times less than that in tidal debris surrounding these two galaxies, we are only viewing this distribution for one snapshot in time. The galactic winds from the LMC could have ejected more than 10% of the total mass and more than 60% of the total metals found in these tidal structures if they have been relatively continuous since the Magellanic Stream was created 1 – 2 Gyr ago (e.g., Besla et al. 2010). As the global star formation activity in the LMC has not been continuous, the galactic winds likely died down when the stellar activity diminished. The global star formation of the LMC peaked at 12 Myr, 100 Myr, 500 Myr, and 2 Gyr with the last two bursts coinciding with a burst star formation in the SMC, suggesting that they were induced by interactions between the two galaxies (Harris & Zaritsky 2009). Surrounding the Magellanic Clouds, we see evidence for multiple outflow episodes with the LMC HVC complex at $v_{\rm LSR} = +130\ \rm km\,s^{-1}$ (see Lehner et al. 2009) and an enriched Magellanic Stream filament (see Richter et al. 2013).

Galactic winds generated by stellar activity have been observed in other galaxies. Martin (1998) detected outflows in 13 out of 15 of their star-forming dwarf galaxies with masses and specific star-formation rates (sSFR) ranging from $8.1 \le \log(M_\star/M_\odot) \le 10.4$ and $5\times10^{-12} \le {\rm sSFR} \le 8\times10^{-10}\ {\rm yr}^{-1}$ (these ranges exclude M82 as it is well-known for having exceptionally strong outflows). By summing together all of the ionized gas mass detected in Hα shells expanding out of the galaxies' disks, they find wind masses of $8\times10^3 \le M_{\rm out}/M_\odot \le 3\times10^6$ that are flowing at a rate of $2\times10^{-3} \le (\dot{M}_{\rm out}/M_\odot\,{\rm yr}^{-1}) \le 2$; these values assume a volume filling factor of $\epsilon = 0.01$, which is consistent for pressure equilibrium conditions between the warm and hot gas in these shells and is expected to be accurate to within a factor of 10 (Martin 1999). The span of their galaxy sample includes galaxies with LMC masses and SFR, where the LMC has $M_\star \approx 3\times10^9\ M_\odot$ (van der Marel et al. 2009) and ${\rm SFR_{LMC}} \lesssim 0.2\ M_\odot\ {\rm yr}^{-1}$ (or ${\rm sSFR} = 2\times10^{-11}\ {\rm yr}^{-1}$) (Harris & Zaritsky 2009). Their outflow masses and rates

are consistent with the values we estimate for the LMC of $M_{\rm out} = 1.3 \times 10^6 M_\odot$ and $\dot{M}_{\rm out} = 4 \times 10^{-2}\ M_\odot\,{\rm yr}^{-1}$, assuming $R_{\rm out} = 3.7$ kpc and $v_{\rm out} = 50\ {\rm km\,s^{-1}}$.

Both of the Magellanic Clouds have lost substantial quantities of metals over their lifetimes. Similarly, substantial metals have been detected around other nearby dwarf galaxies (Bordoloi et al. 2014a and Liang & Chen 2014). Within a distance of one half the virial radius (15 kpc to 100 kpc for galaxy masses $8.5 \leq \log M_\star/M_\odot \leq 10$) and within $150\ {\rm km\,s^{-1}}$ of the systemic velocity of their isolated dwarf galaxy sample, Bordoloi et al. (2014a) found that there is more carbon surrounding these dwarf galaxies than locked in their stellar populations, with carbon masses that exceed 10^6 $M_\odot$. The stark difference in carbon mass between their galaxy sample and the LMC at only few hundred solar masses could be related to the difference in the volume probed where their C IV detections span out to ~ 100 kpc from their galaxies whereas we are likely probing only a few kpc to tens of kpc for the gas within $\sim 100\ {\rm km\,s^{-1}}$ of the LMC (the LMC is 50 kpc away). Extending $R_{\rm out}$ to 100 kpc and assuming that $f_\Omega = 1$ and $\Omega = 2\pi$, the total carbon mass around the LMC would still only be $\sim 1/20$ of that found by the Bordoloi et al. (2014a). However, their observations are tracing the amount carbon that surrounds their galaxies sample regardless of how that material got there and therefore traces multiple pollution processes in addition to outflows. Additionally, the environments of these galaxies are very different—the Magellanic Clouds have lost over 2×10^9 $M_\odot$ due to galaxy interactions (Fox et al. 2014), while the Bordoloi et al. (2014a) galaxies are isolated. Furthermore, any outflows may be further stripped away from the LMC by interactions with the MW corona.

The regions surrounding galaxies have been observed to be a reservoir of gas and metals that is strongly correlated with the star-formation activity within them (e.g., Tumlinson et al. 2011 and Bordoloi et al. 2014a,b). In L^* galaxies, roughly half of the metals (Peeples et al. 2014) and baryons (Werk et al. 2014) exists outside of their disks. Bordoloi et al. (2011) and Rubin et al. (2014) find that the detection rate of the galactic winds is strongly correlated with the inclination angle of the galaxy, where this rate is greatest for near face-on galaxies for a sample of 105 galaxies that spans a mass range of $9.5 \lesssim \log M_\star/M_\odot \lesssim 11.5$ at $z > 0.3$. The LMC is both near face-on and forming stars, but has an outflow rate for the low-ionization species that is more than a magnitude lower than the rate found for the star-forming galaxies in Rubin et al. (2014). However, the LMC is on the low-mass end of their sample and a lower-mass sample of galaxies is needed for a direct comparison with the LMC outflow quantities.

4.3. *The HVC complex toward and around the LMC*

We noted in Section 3.2 that there is detection of a high-velocity absorber at $v_{\rm LSR} \approx +130\ {\rm km\,s^{-1}}$ toward CAL F and HD 33133 (see Figures 3 and 4). The HVC absorption is less prominent along the CAL F sight line as the COS spectrograph has a lower velocity resolution than the STIS spectrograph (see Table 2), but it is present in the C II λ1334, Si II λ1260, 1526, and Si III λ1206 transitions. For this cloud, we measure [Si II/O I] = $+0.25 \pm 0.12$, placing its ionization fraction of the low-ionization gas of $> 55\%$. This HVC is part of the well studied HVC complex toward the LMC at $+90 \lesssim v_{\rm LSR} \lesssim +175\ {\rm km\,s^{-1}}$ that spans at least the angular extent of the LMC with a 70% covering fraction in O I λ1039, Fe II λ1144, and N II λ1083 and 90% in O VI λ1031 (Lehner et al. 2009). It has an ionization fraction that exceeds 50% for the low-ionization species (Lehner et al. 2009), consistent with the ionization level observed toward CAL F and HD 33133.

The HVC at $+90 \lesssim v_{\rm LSR} \lesssim +175\ {\rm km\,s^{-1}}$ has been detected in both H I emission (Staveley-Smith et al. 2003) and UV absorption (Lehner & Howk 2007; Lehner et al. 2009). Several properties of this HVC connected its origin to an outflow from the LMC: (1) Staveley-Smith et al. (2003) found that the regions of this complex with high H I column densities are often projected onto H I voids (such as supergiant shells, e.g., LMC 3) within the LMC disk that connect back to the disk of the LMC with spatial and kinematics bridges (see their Figures 9 and 11). Redman et al. (2003) also found similar bridges in [O III] emission towards the 30 Doradus starburst region (see their Figures 4–6). (2) This complex shows a gradient in its LMC-frame velocity with RA across the entire LMC in both H I emission as well as O I and Fe II absorption (see Figure 5 in Lehner et al. 2009). (3) This HVC complex has a metallicity that is similar to that of the LMC ([O/H] = −0.4; e.g., Russell & Dopita 1992) with [O/H] = $-0.51^{+0.12}_{-0.16}$ (Lehner et al. 2009). And (4) it contains dust based on the depletion of iron relative to silicon (Lehner et al. 2009, and see also Welty et al. 1999; Smoker et al. 2015) in addition to H_2 (Richter et al. 1999), although molecules are not widespread (see Lehner et al. 2009).

However, HVC absorption at $v_{\rm LSR} \approx +150\ {\rm km\,s^{-1}}$ in this general direction has now been detected toward a star for which the distance is estimated to be $d = 9.2^{+4.1}_{-7.2}$ kpc from the Sun (Werner & Rauch 2015). This provides an upper limit on the distance to the HVC complex toward the LMC of < 13 kpc. Clearly, a present-day outflow from the LMC is not a plausible origin anymore in the light of this distance as argued by Richter et al. (2015). However, this HVC complex is quite peculiar compared to the overall HVC population with the presence of dust (uncommon in HVCs; see Wakker & Boulanger 1986 and Wakker 2001). If this HVC complex is not related to the LMC, the kinematic and morphological properties described above that appear to connect it to the LMC would be entirely fortuitous.

It is quite plausible that this complex is just a Milky Way HVC. However, given its peculiarities compared with most HVCs, we explore whether this complex could represent an ancient LMC outflow driven by a burst of star formation some time ago. Assuming an average velocity of 100–150 ${\rm km\,s^{-1}}$, it would take to this gas about 250–400 Myr to travel 40 kpc (ignoring possible drag forces and initial higher velocity). Coincidentally, this travel time corresponds to an epoch when a burst of star formation occurred in the LMC (Harris & Zaritsky 2009). This is quite far for an HVC to travel through the ionizing radiation fields of the surrounding galaxies and through the Milky Way's hot halo. The survival of an HVC is dependent on its size, mass, its initial velocity, as well as if it is shielded by its magnetic field. Heitsch & Putman (2009) show that for typical cloud velocities and halo densities, H I HVCs with masses $< 10^{4.5}$ $M_\odot$ will lose their H I content within 10 kpc or less; however, their remnants could contribute warm ionized HVCs. Armillotta, Fraternali, and Werk (2015, in prep.) are investigating the survival of an HVC with LMC metallicity traveling through the hot MW halo with different initial masses, sizes, and velocities, and early results suggest that massive clouds of $> 10^6$ $M_\odot$ are far more difficult to disrupt than smaller cloud, i.e., they may be able to

survive for several hundreds of Myrs. This is because in the low density gas of the MW halo, both the ram pressure and Kelvin-Helmholtz instability effects are weak, which considerably slows down cloud disruption (see also Fraternali et al. 2015).

If the LMC had a major outflow some 300–400 Myr ago, we would expect that (1) the HVC complex has expanded beyond the disk of the LMC and (2) toward QSOs a higher velocity counterpart corresponding to the receding ancient outflow might be present. While it is beyond the scope of this paper to do a full analysis of the other QSOs in our HST program 11692 and other QSOs since observed with other programs, thanks to the survey by Fox et al. (2014), all these QSO spectra are available. In Table 5, we list QSOs within 20° of the LMC's kinematic center[6] showing high-velocity absorption components (excluding QSOs toward the Magellanic Bridge). In the Fox et al. paper, these QSOs are identified as LMC-On and LMC-Off. As the H I LMC disk radius is about 4.5°, this sample of QSOs allows us to search for high-velocity absorption components well beyond the LMC disk, 2.8° to 19.3° from the LMC center.

To identify absorption at $v_{\rm LSR} > +90$ km s^{-1}, we require that there is absorption at the same velocity for at least two different ions from the following list: Si II, Si III, Si IV, C II, and/or C IV. Within 17° from the LMC center, high-velocity absorption is detected at velocities $+100 \leq v_{\rm LSR} \leq +160$ km s^{-1}, consistent with the HVC complex velocities observed toward the LMC.[7] As noted by Fox et al. (2014), all the QSO sight lines have evidence for LMC halo gas well beyond the disk of the LMC up to 20 kpc at velocities $+260 \lesssim v_{\rm LSR} \lesssim +315$ km s^{-1}. There is also evidence in 4/11 sight lines of very high-velocity absorption at $+360 \lesssim v_{\rm LSR} \lesssim +420$ km s^{-1}. These velocities are quite peculiar, offset by 80–140 km s^{-1} from a systemic velocity of $v_{\rm LSR} = +280$ km s^{-1} (Staveley-Smith et al. 2003; Kim et al. 1998). This offset relative to the LMC systemic velocity is quite similar to the HVC complex velocity difference with the LMC systemic velocity, suggesting that the very high-velocity absorption at $+360 \leq v_{\rm LSR} \leq +420$ km s^{-1} could be the receding component of the ancient LMC outflow while the HVC complex at $+100 \leq v_{\rm LSR} \leq +160$ km s^{-1} could be the approaching component.

The two expected outcomes from an ancient LMC outflow are observed, providing some additional support to the scenario that an ancient LMC outflow may feed the MW lower halo. Although the properties of this high-velocity gas observed towards the LMC have many attributes that are uncommon amongst the Milky Way's cloud population, there is the possibility that it is unrelated to an LMC outflow. However, while the covering fraction of the MW HVCs seen in UV absorption with $90 \lesssim |v_{\rm LSR}| \lesssim 170$ km s^{-1} is quite high, around 60%, the covering fraction of HVC with $|v_{\rm LSR}| > 170$ km s^{-1} is only about 10% when the Magellanic Stream is removed (Lehner et al. 2012); and at these positions, this is unlikely to be Magellanic Stream gas. Future simulations of the travel of high-velocity gas through the MW halo will be able to test the survivability of an HVC complex depending on its initial mass and test if outflows from dwarf galaxies may be one of the sources of the HVC gas seen at 5–20 kpc from the Sun.

[6] $(l, b) = (279.75°, -33.60°)$; Kim et al. (1998).

[7] We note that the anti-correlation between the LMC standard of rest velocity and the R.A. derived by Lehner et al. 2009 also applies to the QSO sight lines at smaller and larger R.A., although with a larger scatter.

In all the above, we have ignored any shear the Galactic halo gas may impart as the LMC and its outflow move through it. The LMC is moving at ~ 300 km s^{-1} relative to the MW (Kallivayalil et al. 2013). If the drag from the halo imparts even a 10 km s^{-1} transverse motion of the outflow relative to the LMC, it will displace it by ~ 4 kpc, or an LMC radius, in 400 Myr. Our earlier suggestion that a lack of inflowing gas may be the result of incorporation of that material into the Galactic corona relies on a similar effect. Thus, it is not clear how an outflow from several hundred Myr ago would maintain its position between us and the LMC. Thus despite being among the best characterized HVC complex with an unprecedented level of information regarding its kinematics, metallicity, ionization and dust structures on both small and large scales, its origin remains uncertain. To make progress we see two ways. From the theoretical side, future hydrodynamical simulations taking into account the relative motion of the LMC and MW may help providing additional clues regarding the origin of this HVC complex. From the observational side, we have started to collect Wisconsin Hα Mapper (WHAM) observations to map in Hα the true spatial and kinematical distributions of the HVC complex. This Hα map will inform us on its overall displacement relative relative to the LMC and geometry, and hence we will be able to reassess its origin and estimate a more accurate mass. Preliminary analysis reveals that this HVC could extend more than 10-degrees from the center of the LMC in the direction of the RBS 542 sight line at $v_{\rm LSR} \approx +175$ km s^{-1} and more than 20-degrees in the direction of the PKS 0558-504 sight line at $v_{\rm LSR} \approx +250$ km s^{-1}, consistent with the absorption listed in Table 5. More analysis will need to be done to determine if the emission in these directions trace the same HVC complex.

We finally note that the mass of this HVC complex toward the LMC can be assessed with its newly measured distance and with a new determination of its sky coverage. This HVC complex is possibly one of the best characterized HVCs thanks to the multitude of background LMC stars used to determine its properties as described above. Following Lehner et al. (2009), the mass of the neutral gas in the outflow can be estimated with $M_{\rm HVC}^{\rm neut} = 1.3 m_{\rm p} f_{\rm cov}\, \overline{N}_{\rm O\,I}\, ({\rm O/H})_{\rm HVC}^{-1}\, A_{\rm HVC}$, where the covering factor is $f_{\rm cov} = 0.7$, the average O I column density is $\overline{N}_{\rm O\,I} \simeq 10^{14.9}$ cm^{-2} (Lehner et al. 2009). For the HVC complex seen only over the LMC disk, but now assuming a distance of 5 kpc from the MW with an area of the HVC is $A_{\rm HVC} \simeq 1.9$ kpc^2, results in a new estimate of $M_{\rm HVC}^{\rm neut} \approx 7 \times 10^4$ M$_\odot$. Here we assume that the HVC spans the surface of a sphere for the area, but note that the geometry is very uncertain and that other reasonable geometries (i.e., rectangular, disk, etc.) could decrease this mass estimate by a factor of 3 (see e.g., values in Richter et al. 2015). Including the photoionized gas probed by Si II and Fe II, the mass would increase by at least another factor 2, and including the O VI would increase the mass by another factor $\gtrsim 2$ (see Lehner et al. 2009), yielding a total mass of $\gtrsim 3 \times 10^5$ M$_\odot$. As discussed above, the HVC complex extends beyond the HVC H I disk by an additional $\sim 10°$ (i.e., $\theta_{\rm dist,\ HVC} \simeq 30°$), implying a total mass of $\gtrsim 3 \times 10^6$ M$_\odot$ assuming that the properties (ionization, metallicity) of the HVC beyond the LMC disk are the same. If the HVC complex toward the LMC is an ancient LMC outflow, and if the initial mass of that ancient outflow was similar to the mass of the present-day mass outflow (see Section 4.2), this would mean that most of the mass of the ancient outflow has been lost before reaching the inner MW

Table 5
Velocity Components with $v_{\rm LSR} \geq +90$ km s^{-1} toward QSOs around the LMC

QSO	g_l (°)	g_b (°)	$\Delta\theta$[a] (°)	Direction[a]	$v_{\rm LSR}$ (km s^{-1})
CAL F	277.2	−35.4	2.8	N	+130, +260, +410
PKS 0552–6402	273.5	−30.6	6.1	NW	+100, +280, +420
2E 0622.9-6434	274.3	−27.3	7.8	NW	+110, +280, +380, +420
RBS 563	272.3	−39.2	8.3	N	+100, +150, +220, +300
PKS 0637–752	286.4	−27.2	8.6	SE	+110, +240, +320
RBS 542	267.0	−42.0	13.1	NW	+100, +160, +310, +360
HE 0429–5343	262.1	−42.2	16.3	NW	+100, +280
RBS 567	261.2	−40.9	16.4	NW	+100, +220, +280, +315
HE0 435–5304	261.0	−41.4	16.7	NW	+100, +280
HE0 439–5254	260.7	−40.9	16.8	NW	+100, +280
PKS 0558–504	258.0	−28.6	19.3	NE	+265

[a] Angular separation and approximate direction from the LMC center.

halo. As described above, ongoing and future WHAM observations will allow us to better define the geometry and extent of this HVC complex, and hence to more accurately determine its mass.

5. SUMMARY

We have investigated the gas surrounding the LMC by comparing the absorption along a star embedded within its disk (target HD 33133) with a background AGN (target CAL F). These targets are only 7.2′ apart on the sky (corresponding to a projected physical separation of 105 pc), which enables us to probe similar large-scale environment along these sight lines and to separate the gas flows on the near and far side of the galaxy's disk. Using UV spectroscopic *HST* observations, we show that gaseous material is flowing away from both sides of the H I disk of the LMC in Section 4.2. From the strikingly similar properties of the near and far side gaseous outflows along the neighboring HD 33133 and CAL F sight lines, the detection of similar intermediate-velocity absorption with high $N_{\rm C\,IV}/N_{\rm Si\,IV}$ ratio toward stars spread across the LMC in Lehner & Howk (2007), and the scarcity of inflowing material observed in Howk et al. (2002) toward stars also scattered throughout the disk, we conclude that a pervasive wind expels a large amount of predominantly ionized gas from the disk of the LMC. The outflowing material within ∼100 km s^{-1} of the LMC has the following properties:

1. **Kinematics:** We observe a kinematically continuous, multiphase gas that is made up of neutral gas and low- and high-ionization species that extends further than the kinematic extent of the H I disk of the LMC. This material is flowing away from the LMC's disk with speeds up to −100 km s^{-1} on the near side and +100 km s^{-1} on the far side of the galaxy. The absorption is very broad, having breadths large enough to require significant non-thermal motions (see Figures 8 and 7).

2. **Ionization Fraction:** The warm intermediate-velocity gas ($v_{\rm LMC} = \pm 100$ km s^{-1}) on both sides of the LMC has an ionization fraction that exceeds 72% ([Si II/O I] = +0.50 ± 0.08; see Section 3.3). The ionization fraction of the highly-ionized gas at greater temperatures likely approaches unity.

3. **Ionization Sources:** The gas is multiphase with the low ions being most certainly photoionized. The high ions (Si IV and C IV) have been predominantly ionized through collisional processes as evidenced by their broad and smooth velocity structure and an ionic ratio of $N_{\rm C\,IV}/N_{\rm Si\,IV} \approx 3.5$ (see Section 3.3).

4. **Baryonic Mass and Mass-Loss Rate:** We estimate the mass and mass-loss rates of the intermediate-velocity gas within 100 km s^{-1} of the LMC at 1.5×10^7 M$_\odot$ $(R_{\rm out}/3.7$ kpc$)^2$ and 4.1×10^{-1} M$_\odot$ yr^{-1}$(v_{\rm out}/50$ km s^{-1}) in the low-ionization state and $> 1.4 \times 10^6$ M$_\odot$ $(R_{\rm out}/3.7$ kpc$)^2$ and $> 4.0 \times 10^{-2}$ M$_\odot$ yr^{-1} $(v_{\rm out}/50$ km s^{-1}) in high-ionization state. The low ions dominate the mass contribution for the gas-phases explored in this study.

5. **Metal Mass and Mass-Loss Rate:** We found that the LMC galactic wind is ejecting more than 8.0×10^4 M$_\odot$ $(R_{\rm out}/3.7$ kpc$)^2$ from the LMC disk at a rate exceeding 2.2×10^{-3} M$_\odot$ yr^{-1} $(R_{\rm out}/3.7$ kpc$)$ $(v_{\rm out}/50$ km s^{-1}) in the low- and high-ionization states. These value will increase if these outflows contain metal enriched gas compared to the present-day metallicity of the LMC.

Because the sight lines in this study probe a relatively quiescent region of the LMC (Figure 1), the intermediate-velocity absorbing material they trace at $v_{\rm LMC} = \pm 100$ km s^{-1} was likely expelled by stellar feedback in the highly active star-forming regions of the LMC (Section 4.1). In this scenario, the outflows become thermalized and have expanded across the disk, making them detectable far from where they were ejected. The LMC has therefore undergone at least one major outflow that coincides with the recent intense stellar activity (Harris & Zaritsky 2009). While the velocity of this outflow is smaller than the escape velocity, most of the outflowing material appears to escape into the MW since there is little evidence of infalling gas (Howk et al. 2002; Lehner & Howk 2007). The removal of these outflows is likely aided by tidal interactions between the SMC and MW and ram-pressure stripping with the Galactic halo (Hammer et al. 2015; Salem et al. 2015), implying that the environment of galaxies could play an important role in the gas starvation of LMC-like or dwarf galaxies.

We thank Y.-H. Chu for providing us with the reduced 2D Hα spectrum of HD 33133 from Chu et al. (1999) as well as Lister Staveley-Smith and Sungeun Kim for providing us with the ATCA and Parkes telescopes LMC H I survey datacube. We also acknowledge useful discussions

with Tony Wong and Gurtina Besla and comments made by the anonymous referee. This paper includes archived H I LMC data obtained through the Australia Telescope Online Archive (http://atoa.atnf.csiro.au) and the Galactic All Sky Survey Archive (http://www.atnf.csiro.au/research/GASS). This paper also includes archived FUSE data available through the Mikulski Archive for Space Telescopes (MAST: http://archive.stsci.edu). Support for this program was provided by NASA through through the grant HST-GO-11692 from the Space Telescope Science Institute, which is operated by the Association of Universities for Research in Astronomy, Incorporated, under NASA contract NAS5-26555. K.A. Barger was supported through NSF Astronomy and Astrophysical Postdoctoral Fellowship award AST 1203059.

REFERENCES

Asplund, M., Grevesse, N., Sauval, A. J., & Scott, P. 2009, ARA&A, 47, 481
Barger, K. A., Haffner, L. M., & Bland-Hawthorn, J. 2013, ApJ, 771, 132
Barger, K. A., Madsen, G. J., Bland-Hawthorn, J., Nidever, D. Fox, A. J., Wakker, B. P., & Haffner, L. M. 2014, in Prep.
Besla, G., Kallivayalil, N., Hernquist, L., van der Marel, R. P., Cox, T. J., & Kereš, D. 2010, ApJL, 721, L97
Bordoloi, R., et al. 2011, ApJ, 743, 10
—. 2014a, ApJ, 796, 136
—. 2014b, ApJ, 794, 130
Bostroem, K. A., & Proffitt, C. 2011, STIS Data Handbook v. 6.0
Bowen, D. V., Jenkins, E. B., Pettini, M., & Tripp, T. M. 2005, ApJ, 635, 880
Boylan-Kolchin, M., Bullock, J. S., Sohn, S. T., Besla, G., & van der Marel, R. P. 2013, ApJ, 768, 140
Brüns, C., et al. 2005, A&A, 432, 45
Chu, Y.-H., Weis, K., & Garnett, D. R. 1999, AJ, 117, 1433
Danforth, C. W., & Blair, W. P. 2006, ApJ, 646, 205
Danforth, C. W., Howk, J. C., Fullerton, A. W., Blair, W. P., & Sembach, K. R. 2002, ApJS, 139, 81
Erb, D. K., Quider, A. M., Henry, A. L., & Martin, C. L. 2012, ApJ, 759, 26
Fox, A. J., Ledoux, C., Petitjean, P., & Srianand, R. 2007, A&A, 473, 791
Fox, A. J., et al. 2014, ApJ, 787, 147
Fraternali, F., Marasco, A., Armillotta, L., & Marinacci, F. 2015, MNRAS, 447, L70
Froning, C. S., & Green, J. C. 2009, Ap&SS, 320, 181
Gardiner, L. T., & Noguchi, M. 1996, MNRAS, 278, 191
Gaustad, J. E., McCullough, P. R., Rosing, W., & Van Buren, D. 2001, PASP, 113, 1326
Gnat, O., & Sternberg, A. 2007, ApJS, 168, 213
—. 2009, ApJ, 693, 1514
Green, J. C., et al. 2012, ApJ, 744, 60
Hammer, F., Yang, Y. B., Flores, H., Puech, M., & Fouquet, S. 2015, ApJ, 813, 110
Harris, J., & Zaritsky, D. 2009, AJ, 138, 1243
Heald, G. H., Rand, R. J., Benjamin, R. A., & Bershady, M. A. 2007, ApJ, 663, 933
Heckman, T. M., Armus, L., & Miley, G. K. 1990, ApJS, 74, 833
Heckman, T. M., Lehnert, M. D., Strickland, D. K., & Armus, L. 2000, ApJS, 129, 493
Heitsch, F., & Putman, M. E. 2009, ApJ, 698, 1485
Holland, S. T., & et al. 2014, Cosmic Origins Spectrograph Instrument Handbook v. 6.0
Howk, J. C., Sembach, K. R., Savage, B. D., Massa, D., Friedman, S. D., & Fullerton, A. W. 2002, ApJ, 569, 214
Kacprzak, G. G., Churchill, C. W., Barton, E. J., & Cooke, J. 2011, ApJ, 733, 105
Kacprzak, G. G., et al. 2014, ApJL, 792, L12
Kafle, P. R., Sharma, S., Lewis, G. F., & Bland-Hawthorn, J. 2014, ApJ, 794, 59
Kalberla, P. M. W., Burton, W. B., Hartmann, D., Arnal, E. M., Bajaja, E., Morras, R., & Pöppel, W. G. L. 2005, A&A, 440, 775
Kalberla, P. M. W., et al. 2010, A&A, 521, A17
Kallivayalil, N., van der Marel, R. P., & Alcock, C. 2006, ApJ, 652, 1213
Kallivayalil, N., van der Marel, R. P., Besla, G., Anderson, J., & Alcock, C. 2013, ApJ, 764, 161
Kamphuis, P., Peletier, R. F., Dettmar, R.-J., van der Hulst, J. M., van der Kruit, P. C., & Allen, R. J. 2007, A&A, 468, 951
Kim, C.-G., & Ostriker, E. C. 2015, ApJ, 802, 99
Kim, S., Dopita, M. A., Staveley-Smith, L., & Bessell, M. S. 1999, AJ, 118, 2797
Kim, S., Staveley-Smith, L., Dopita, M. A., Freeman, K. C., Sault, R. J., Kesteven, M. J., & McConnell, D. 1998, ApJ, 503, 674
Kim, S., Staveley-Smith, L., Dopita, M. A., Sault, R. J., Freeman, K. C., Lee, Y., & Chu, Y.-H. 2003, ApJS, 148, 473
Knauth, D. C., Howk, J. C., Sembach, K. R., Lauroesch, J. T., & Meyer, D. M. 2003, ApJ, 592, 964
Kurt, C. M., & Dufour, R. J. 1998, in Revista Mexicana de Astronomia y Astrofisica, vol. 27, Vol. 7, Revista Mexicana de Astronomia y Astrofisica Conference Series, ed. R. J. Dufour & S. Torres-Peimbert, 202
Kwak, K., & Shelton, R. L. 2010, ApJ, 719, 523
Lehner, N., & Howk, J. C. 2007, MNRAS, 377, 687
Lehner, N., Howk, J. C., Keenan, F. P., & Smoker, J. V. 2008, ApJ, 678, 219
Lehner, N., Howk, J. C., Thom, C., Fox, A. J., Tumlinson, J., Tripp, T. M., & Meiring, J. D. 2012, MNRAS, 424, 2896
Lehner, N., Howk, J. C., & Wakker, B. P. 2015, ApJ, 804, 79
Lehner, N., Staveley-Smith, L., & Howk, J. C. 2009, ApJ, 702, 940
Lehner, N., Zech, W. F., Howk, J. C., & Savage, B. D. 2011, ApJ, 727, 46
Liang, C. J., & Chen, H.-W. 2014, MNRAS, 445, 2061
Martin, C. L. 1998, ApJ, 506, 222
—. 1999, ApJ, 513, 156
McClure-Griffiths, N. M., et al. 2009, ApJS, 181, 398
Morton, D. C. 2003, ApJS, 149, 205
Nidever, D. L., Majewski, S. R., & Burton, W. B. 2008, ApJ, 679, 432
Oosterloo, T., Fraternali, F., & Sancisi, R. 2007, AJ, 134, 1019
Oppenheimer, B. D., & Schaye, J. 2013, MNRAS, 434, 1043
Pathak, A., Pradhan, A. C., Sujatha, N. V., & Murthy, J. 2011, MNRAS, 412, 1105
Peeples, M. S., Werk, J. K., Tumlinson, J., Oppenheimer, B. D., Prochaska, J. X., Katz, N., & Weinberg, D. H. 2014, ApJ, 786, 54
Putman, M. E., et al. 1998, Nature, 394, 752
Redman, M. P., Al-Mostafa, Z. A., Meaburn, J., & Bryce, M. 2003, MNRAS, 344, 741
Richter, P., de Boer, K. S., Werner, K., & Rauch, T. 2015, ArXiv e-prints
Richter, P., de Boer, K. S., Widmann, H., Kappelmann, N., Gringel, W., Grewing, M., & Barnstedt, J. 1999, Nature, 402, 386
Richter, P., Fox, A. J., Wakker, B. P., Lehner, N., Howk, J. C., Bland-Hawthorn, J., Ben Bekhti, N., & Fechner, C. 2013, ApJ, 772, 111
Rubin, K. H. R., Prochaska, J. X., Koo, D. C., Phillips, A. C., Martin, C. L., & Winstrom, L. O. 2014, ApJ, 794, 156
Rubin, K. H. R., Weiner, B. J., Koo, D. C., Martin, C. L., Prochaska, J. X., Coil, A. L., & Newman, J. A. 2010, ApJ, 719, 1503
Russell, S. C., & Dopita, M. A. 1992, ApJ, 384, 508
Salem, M., Besla, G., Bryan, G., Putman, M., van der Marel, R. P., & Tonnesen, S. 2015, ArXiv e-prints
Sancisi, R., Fraternali, F., Oosterloo, T., & van der Hulst, T. 2008, A&A Rev., 15, 189
Savage, B. D., & Sembach, K. R. 1991, ApJ, 379, 245
Slavin, J. D., Shull, J. M., & Begelman, M. C. 1993, ApJ, 407, 83
Smoker, J. V., Fox, A. J., & Keenan, F. P. 2015, MNRAS, 451, 4346
Stanimirović, S., Staveley-Smith, L., & Jones, P. A. 2004, ApJ, 604, 176
Staveley-Smith, L., Kim, S., Calabretta, M. R., Haynes, R. F., & Kesteven, M. J. 2003, MNRAS, 339, 87
Stocke, J. T., Keeney, B. A., Danforth, C. W., Shull, J. M., Froning, C. S., Green, J. C., Penton, S. V., & Savage, B. D. 2013, ApJ, 763, 148
Tumlinson, J., et al. 2011, Science, 334, 948
van der Marel, R. P., Alves, D. R., Hardy, E., & Suntzeff, N. B. 2002, AJ, 124, 2639
van der Marel, R. P., Kallivayalil, N., & Besla, G. 2009, in IAU Symposium, Vol. 256, IAU Symposium, ed. J. T. Van Loon & J. M. Oliveira, 81–92
Veilleux, S., Cecil, G., Bland-Hawthorn, J., Tully, R. B., Filippenko, A. V., & Sargent, W. L. W. 1994, ApJ, 433, 48
Wakker, B. P. 2001, ApJS, 136, 463
Wakker, B. P., & Boulanger, F. 1986, A&A, 170, 84
Wakker, B. P., & Savage, B. D. 2009, ApJS, 182, 378
Walker, A. 1999, Post-Hipparcos Cosmic Candles, 237, 125
Weiner, B. J., et al. 2009, ApJ, 692, 187
Welty, D. E., Frisch, P. C., Sonneborn, G., & York, D. G. 1999, ApJ, 512, 636
Werk, J. K., et al. 2014, ApJ, 792, 8
Werner, K., & Rauch, T. 2015, ArXiv e-prints
Zech, W. F., Lehner, N., Howk, J. C., Dixon, W. V. D., & Brown, T. M. 2008, ApJ, 679, 460

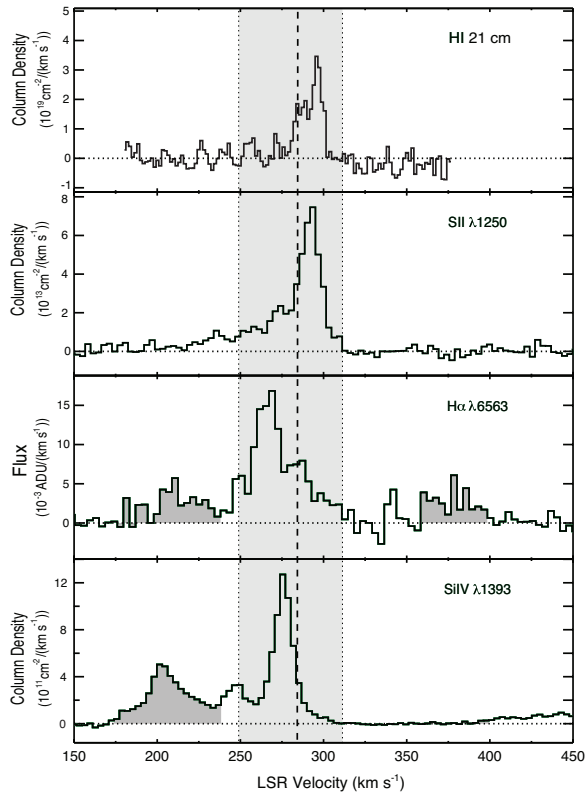

Figure 10. Comparison of emission- and absorption-lines along the HD 33133 sight line. The H I emission and the S II λ1250 species trace the cooler gas phase in the top two panels. The combined ATCA and Parkes H I spectrum traces the small scale structure with an angular resolution of $6'$ (top panel). The Hα emission and SiIV λ1393 species trace the warmer gas (bottom two panels). We extracted the Hα spectrum from a long-slit echelle spectrograph image positioned east-to-west across HD 33133 with a slit width of $1.64''$; Chu et al. (1999) shows this long-slit image, acquired with the 4 – m telescope and the Tektronic detector at the Cerro Tololo Inter-American Observatory (CTIO), in Figure 2 (labeled under the alias Br 13). The grey highlighted components span the velocity extent of the approaching ($+175 \leq v_{\rm LSR} \leq +237$ km s^{-1}) and receding ($+335 \leq v_{\rm LSR} \leq +400$ km s^{-1}) walls of the H II shell surrounding this WR star. To emphasize component structure of this shell, the average Hα spectrum is offset slightly offset from HD 33133, spanning 2.6 to $6.5''$ to the west. The S II λ1250 and Si IV λ1393 apparent column density profiles are only sensitive to the gas in the foreground of HD 33133, whereas the H I and Hα emission is sensitive to both the approaching gas in the foreground and the receding gas in the background. The systemic velocity of the LMC at $v_{\rm LSR} = +282$ km s^{-1} ($v_{\rm LMC} = 0$ km s^{-1}) is marked with a black-dashed line. The extent of H I emission from the LMC disk is highlighted in light grey over the $+250 \leq v_{\rm LSR} \leq +310$ km s^{-1} ($-32 \leq v_{\rm LMC} \leq +28$ km s^{-1}) velocity range as illustrated in Figure 5.

6. APPENDIX

6.1. *Wind Nebula surrounding the HD 33133 stellar target*

The WR star HD 33133 has created a wind nebula as seen from the Hα spatial distribution in the bottom-right panel of Figure 1. The Hα emission spectrum shown in Figure 10 (Chu et al. 1999) also traces this nebula, where the approaching and receding shells are highlighted at $+175 \lesssim v_{\rm LSR} \lesssim +237$ km s^{-1} and $+335 \lesssim v_{\rm LSR} \lesssim +400$ km s^{-1}, respectively. Unlike the absorption spectra along this sight line, the emission traces the entire galaxy and its surroundings. Because the S II λ1250 and Si IV λ1393 apparent column density profiles—also included in this figure—only trace the absorbing material in front of the star, the receding shell is absent in the stellar spectrum.

The high-ion absorption along the stellar HD 33133 sight line shows distinct, narrow components, whereas the absorption along the AGN CAL F sight line only consists of broad velocity components. In Section 3.2 and in Figure 8, we showed that the narrow component structure of the HD 33133 sight line was not due to the differences in the spectral resolution of the COS and STIS instruments. The narrow components in the Si IV spectrum (and in the spectra of other species) near $v_{\rm LSR} \approx +200$ km s^{-1} aligns well with the approaching Hα shell that surrounds this WR star (see Figures 1 and 10). These narrow components indicate that the gas along the HD 33133 sight line is being illuminated by this early-type star and the underlining broad components, similar to those seen along the AGN sight line, suggests that collisional processes also influence this gas. The lack of narrow component structure in the CAL F spectra implies that this sight line lies outside of any hot stars' direct influence.

Because of the low signal-to-noise ratio of the C IV absorption along the HD 33133, we are unable to directly compare the properties of its broad components with those along the CAL F sight line. However, they both appear to have similar underlining properties with both being highly ionized at $x(H^+) \geq 0.72$ in the low-ionization species and likely near unity for the high-ionization species, which are also predominantly collisionally ionized. This suggests that the broad components along these sight lines likely trace the same gas over similar path lengths as these sight lines are projected only 105 pc apart and are affected by the same large-scale processes. Because the underlying broad components seen in C IV along the HD 33133 sight line it is blue shifted with respect to the systemic velocity of the LMC. Therefore, this gas must be flowing towards us on the near side of the galaxy. As the CAL F sight line has an additional red shifted component, that sight line also traces outflowing gas receding from us and the LMC on the far side of the galaxy.